Optimal Mass Distribution Prediction for Human Proximal Femur with Bi-modulus Property

Jiao Shi[*], Kun Cai[*] and Qing H. Qin[†,‡]

Abstract: Simulation of the mass distribution in a human proximal femur is important to provide a reasonable therapy scheme for a patient with osteoporosis. An algorithm is developed for prediction of optimal mass distribution in a human proximal femur under a given loading environment. In this algorithm, the bone material is assumed to be bi-modulus, i.e., the tension modulus is not identical to the compression modulus in the same direction. With this bi-modulus bone material, a topology optimization method, i.e., modified SIMP approach, is employed to determine the optimal mass distribution in a proximal femur. The effects of the difference between two moduli on the final material distribution are numerically investigated. Numerical results obtained show that the mass distribution in bi-modular bone materials is different from that in traditional isotropic material. As the tension modulus is less than the compression modulus for bone tissues, the amount of mass required to support tension loads is greater than that required by isotropic material for the same daily activities including one-leg stance, abduction and adduction.

Keywords: Topology optimization, bi-modulus material, proximal femur, bone remodeling.

1 Introduction

It is recognized that bone illness such as osteoporosis exists widely in aged people. A person with serious osteoporosis is at risk of fracture of bone. Developing an efficient therapy of osteoporosis, in particular a method to improve the speed of bone apposition, is therefore of great significance. To this end, it is useful to investigate the relationship between mass distribution and the mechanical properties of either

[*] College of Water Resources and Architectural Engineering, Northwest A&F University, Yangling 712100, P.R. China.

[†] Research School of Engineering, the Australian National University, ACT 2601, Australia.

[‡] Corresponding author. E-mail: qinghua.qin@anu.edu.au

cortical or cancellous bone. It is noted that Wolff's law [1] is a widely accepted concept which states that the layout of trabecular bone (see the micro-structure of a proximal femur shown in Figure 1) tends to align with the stress field. Thus, researchers have considered that bone tissue in an optimal structure always uses minimum mass to support maximum mechanical loads in accordance with Wolff's law

Wolff's law has been experimentally and numerically investigated during the last 40 years [2-9]. One objective of these studies had been to reveal whether the bone modeling process can finally attain a globally optimized structure. Hollister et al. [10] gave a negative answer. The main reasons for this conclusion may be the use of the coarse mechanics model of bone and the computational conditions of the time. In contrast, an analytical parametric micro-structural model for trabecular bone in proximal femur was presented by Fernandes et al. [11] according to the homogenization theory and optimal densities and orientations were obtained by topology optimization [12]. Kowalczyk [13] used an orthotropic material model to simulate the remodeling process of cancellous bone and showed the optimal micro-structures of bone tissues. Kim and Kwak [14] used a design space optimization (DSO) method to give the optimal micro-structure prediction of the proximal femur. Jang and Kim [15] quantitatively studied Wolff's law with trabecular architecture by a topology optimization method. They stated that topology optimization with minimal structural compliance of femur and bone remodeling with strain energy density (SED) distributed uniformly is equivalent. Cai et al. [16] presented a bionic topology optimization method for continuum design according to Wolff's law.

It should be mentioned that an obvious difference exists between the tension modulus and the compression modulus of either cortical bone or cancellous bone. Yet this difference has not attracted much attention from researchers. In 2006, Zhu et al. [17] investigated the tension and compression modulus of Takin femoral cortical bone. Their results showed that the compression modulus of bone is about 5-6 times of the tensile modulus. This finding implies that bone shows clearly bi-modular behavior. Recently, Cory et al. [18] and Nazarian et al. [3] also gave support to the existence of the difference in other various bones. But there is still no report of prediction of the bone remodeling process in the proximal femur with bi-modulus behavior. The main purpose of the present work is to investigate the optimal material distribution in the human proximal femur subjected to specified loads (for example, load induced by physical motions). To this end, a material replacement method [19, 20] is developed to obtain the optimal material layout in the proximal femur under a given environment.

2 Material Properties

2.1 Bi-modular behavior of elastic material

The stress-strain curve of a bi-modular material is shown in Figure 2. The tension modulus of material is $E_T = \tan\alpha$, and the compression modulus is $E_C = \tan\beta$. The ratio between the two moduli is denoted by $R = E_T/E_C$. As the property of bi-modular material is stress-dependent, it is highly nonlinear (or piecewise linear). In deformation analysis, for the sake of convenience the material property is usually approximated with a differentiable curve [21]. Recently, Cai et al. [19, 20], used the piecewise linear (see Figure 2) relationship and the material replacement operation to perform deformation analysis. In particular, the bi-modular material is replaced by two isotropic materials and the selection between them is based on the stress status at the corresponding point. It is a simplification of the method [22, 23], which enable us to treat the material as an orthotropic material whose moduli (E_x and E_y here) depend on the local stress state. Generally it can be treated as an isotropic materials (if all principal stresses are positive or negative) or orthotropic material (if the first principal stress σ_1 and the third principal stress σ_3 are in opposite sign. In this case the Young's moduli E_1 and E_3 may be different). Actually, the constitutive of material should be transversely isotropic (a kind of orthotropic) in a general case.
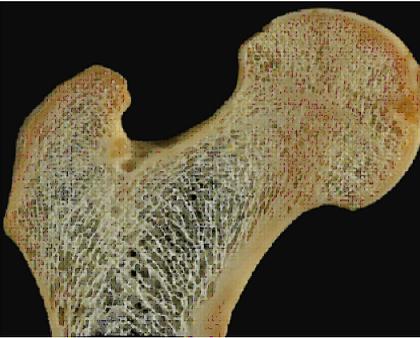
Figure 1: Photograph and radiograph of human proximal femur [24].
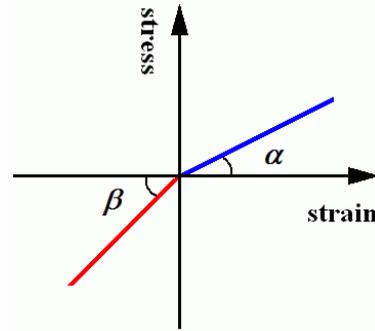
Figure 2: The stress-strain curve of a bi-modular material, $\alpha \neq \beta$.

2.2 Elasticity of porous material

For a porous material, the relationship between the elastic tensor and the relative density is defined as

$$D_{m,ijkl} = \rho_m^p D_{0,ijkl} \tag{1}$$

where $D_{m,\,ijkl}$ is the elastic tensor of the porous material at the m-th point or in the m-th finite element in structure, and its relative density is $\rho_m \in \left[\; 0, \quad 1.0 \;\right]$. p is a material constant. In this work, p is taken to be 2, as suggested by [25]. $D_{0,\,ijkl}$ is the elastic tensor of the corresponding solid material.

3   Optimization model

3.1   *Formulations of topology optimization problem*

During the past decade, the method of continuum topology optimization has been considerably improved and has now become a highly efficient and well-established computational tool for structural design. In contrast to the traditional optimization method, the material in the design domain can vary arbitrarily in topology optimization. So far, several popular topology optimization methods have been published, including the homogenization design method (HDM) [12], the solid isotropic micro-structures with penalization (SIMP) method [26, 27], the evolutionary structural optimization (ESO) method [28], and the level set method [29], widely used in various design fields.

In the present study, the modified SIMP method is employed to determine the relative density distribution of bi-modular bone in the proximal femur with a given amount of mass. Making use of this method, the volume constrained optimization model of a structure with minimal structural mean compliance under multiple loading cases can be expressed as

$$\min_{\{\rho_m\}} c = \sum_{i}^{N} w_i \mathbf{U}_i^T \overline{\mathbf{K}}_i \mathbf{U}_i = \sum_{i}^{N} w_i \sum_{m=1}^{M} \left(\mathbf{u}_m^T \overline{\mathbf{k}}_m \mathbf{u}_m \right)_i$$

$$\text{s.t.}\quad V = \sum_{i}^{N} \sum_{m=1}^{M} \left(\rho_m v_m \right)_i - f_v \cdot V_0 = 0 \tag{2}$$

$$\mathbf{K}_i \mathbf{U}_i = \mathbf{P}_i \ , \ i = 1,\, 2, \cdots ,\, N$$

$$0 < \rho_{\min} \le \rho_m \le 1.0 \ , \ m \in \Omega$$

where the objective function c is the sum of the structural mean compliances under N loading cases. w_i is the weighted coefficient for the i-th loading case. M is the total number of finite elements in the femur. $\{\rho_m\}$ is the set of relative densities of elements. $\mathbf{U}_i$ and $\mathbf{P}_i$ are the global nodal displacement and force vectors in the i-th loading case, respectively. $\overline{\mathbf{k}}_m$ is the modified matrix of $\mathbf{k}_m$(the stiffness matrix of the m-th element with isotropic material, which can be obtained using finite element methods [30-34] by considering bi-modular material behavior. The global stiffness matrix of the structure, $\mathbf{K}_i$, corresponds to the local stiffness matrix $\{\mathbf{k}_m\}_i$ and the modified global stiffness matrix $\overline{\mathbf{K}}_i$ of the structure corresponds to the local

stiffness matrix $\left\{\bar{\mathbf{k}}_m\right\}_i$. $\mathbf{u}_m$ is the nodal displacement vector of the *m*-th element. v_m is the volume of the *m*-th element. f_v is the allowable volume ratio of the final structure. V_0 is the total volume of design domain.

3.2 Update of elastic modulus of local material

In this work, the stress-strain relationships of bone material are defined through Figure 2. The original bi-modular material shown in Figure 2 is replaced by two isotropic materials. The material constitutive relation of the bi-modular material is then determined by the local stress status, i.e., a different stress state may lead to a different elastic tensor. On the other hand, the mechanical behavior of the structure is determined by the distribution of the local stiffness, which is related to the SED [19]. Therefore, the update of the elastic modulus of an element is obtained using the following formulation:

$$E_m = \begin{cases} E_T, & \text{if } (\text{TSED} > \text{CSED})_m \\ E_C, & \text{if } (\text{TSED} < \text{CSED})_m \\ \max(E_T, E_C), & \text{others} \end{cases} \tag{3}$$

where the TSED is the tension SED and CSED is the compression SED. These values can be calculated using the equations

$$\begin{aligned} \text{TSED}_m &= \tfrac{1}{4} \sum_{i=1}^{N} \sum_{j=1}^{3} \left(\sigma_{ji} + \left| \sigma_{ji} \right| \right) \cdot \varepsilon_{ji} \\ \text{CSED}_m &= \tfrac{1}{4} \sum_{i=1}^{N} \sum_{j=1}^{3} \left(\sigma_{ji} - \left| \sigma_{ji} \right| \right) \cdot \varepsilon_{ji} \end{aligned} \tag{4}$$

where σ_{ji} (j=1, 2, 3) and ε_{ji} (j=1, 2, 3) are the mean principal stresses and strains of the *m*-th element, respectively.

3.3 Update of relative density of porous bone

The optimality criteria method [35] is used to determine the increment of relative densities of porous bone tissue in proximal femur. For a given element, say the *m*-th element, the equation for updating relative density is written as

$$\rho_m^{(k+1)} = \begin{cases} \max\left\{ \rho_{\min}, \rho_m^{(k)} - t \right\} & \text{for } \rho_m^{(k)} \Gamma_m^\omega \leq \max\left\{ \rho_{\min}, \rho_m^{(k)} - t \right\} \\ \rho_m^{(k)} \Gamma_m^\omega & \text{others} \\ \min\left\{ 1.0, \rho_m^{(k)} + t \right\} & \text{for } \rho_m^{(k)} \Gamma_m^\omega \geq \min\left\{ 1.0, \rho_m^{(k)} + t \right\} \end{cases} \tag{5}$$

where t is the maximum increment of the design variable ($t = 0.1$ is used in the present study), and ω is a constant (ω=0.5 in this analysis). Γ_m is defined by

$$\Gamma_m = \left| \frac{\partial c}{\partial \rho_m} \bigg/ \left(\lambda \frac{\partial V}{\partial \rho_m} \right) \right|^{(k)} \tag{6}$$

where positive scalar λ is the Lagrangian multiplier which can be obtained using a bi-sectioning algorithm, and

$$\frac{\partial c}{\partial \rho_m} = \sum_{i=1}^{N} -w_i \left(f_m \cdot \frac{p}{\rho_m} \cdot u_m^T \cdot k_m \cdot u_m \right)_i \tag{7}$$

with the modification factor for material replacement operation being defined as

$$f_m = \max \left(10^{-6}, \frac{\text{SED}_m^{\text{effective}}}{\max \left(10^{-30}, \text{TSED}_m + \text{CSED}_m \right)} \right) \tag{8}$$

In Eq (8), $\text{SED}_m^{\text{effective}}$ is the SED of the element defined by the original bi-modular material and under the current stress state.

3.4 *Flowchart of the present algorithm*

Step 1   Build the finite element model of proximal femur and initiate parameters of algorithm; let iteration number k=0.

Step 2   Perform structural analysis to obtain the detailed displacement, strain and stress fields;

Step 3   For each element, update the modulus (Eq.(3)), calculate modification factor (Eq.(8)), update the relative density (Eq.(5));

Step 4   If $k > 10$ and $\left| \frac{c_k - c_{k-j}}{c_k} \right| < 0.001$ (j=1, 2, 3, 4), go to Step5;

Step 5   If k=40, go to Step 6; else k=k+1, go to Step 2;

Step 6   Stop.

4   Numerical results and discussions

In this section, two cases of bone tissues (one isotropic and the other bi-modular) are considered to demonstrate the applicability, numerical accuracy, and effects of the percentage of materials on material distribution. The commercial software ANSYS [36] is adopted to provide numerical results of the deformation of the

(a) load case 1   (b) load case 2   (c) load case 3
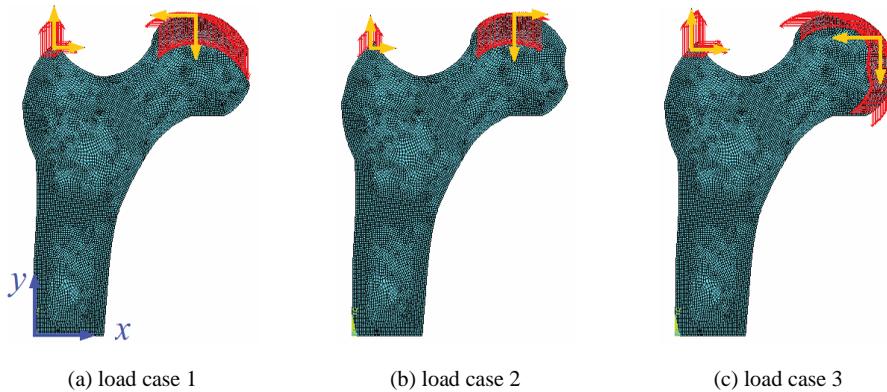
Figure 3: Three loading cases for daily activities: (a) One-legged stance, (b) abduction, (c) adduction. The bottom of the femur is constrained in all directions. (Red arrows show the distribution area of pressure and yellow arrows stand for the directions of force components.)

proximal femur for optimization analysis. The finite element mesh used in this work is shown in Figure 3.

In Figure 3, the upper part of the proximal femur is discretized with 9240 four-node plane stress elements. The relative density of the bone varies within the range of [0.05, 1.0]. The bottom is simply supported in all directions. In this study, cortical bone with the elastic compressive modulus of 17.0 Gpa and Poisson's ratio of 0.3 is considered The modulus of the bone under tension is less than that under compression. The ratio of tension modulus to compression modulus is assumed to be R=0.2, 0.4, 0.6, 1.0(isotropic material). When R is not equal to 1.0, the material is bi-modular. Three volume ratios of the proximal femur (35%, 41% and 46%) are considered in this section.

Table 1: Forces in three load cases in the proximal femur model.

Load case	Cycles/day	Abductor reaction force		Joint reaction force	
		Magnitude/N	Orientation/°	Magnitude/N	Orientation/°
1 (one-legged stance)	6000	703	28	-2317	24
2 (abduction)	2000	351	-8	-1158	-15
3 (adduction)	2000	468	35	-1548	56

Table 1 lists the data of the forces and orientations applied to the femur. In total 10000 cycles, there are 6000 cycles of one-leg stance, 2000 cycles of abduction and 2000cycles of adduction. Hence, the three loading cases are then weighted by the weighted coefficients 0.6, 0.2 and 0.2, respectively. The sign of each force component is determined according to the assumed coordinate system. The orientation of a force is defined by the angle between the force direction and positive x-axis. The sign of the angle is positive if from positive x-axis to force direction is in the counterclockwise direction. (see Figure 3). Negative force means compressive force and positive means tensile force [15].

4.1   Numerical results for bone with isotropic material

(a) 35%, over 40 iterations   (b) 41%, over 40 iterations   (c) 46%, over 40 iterations
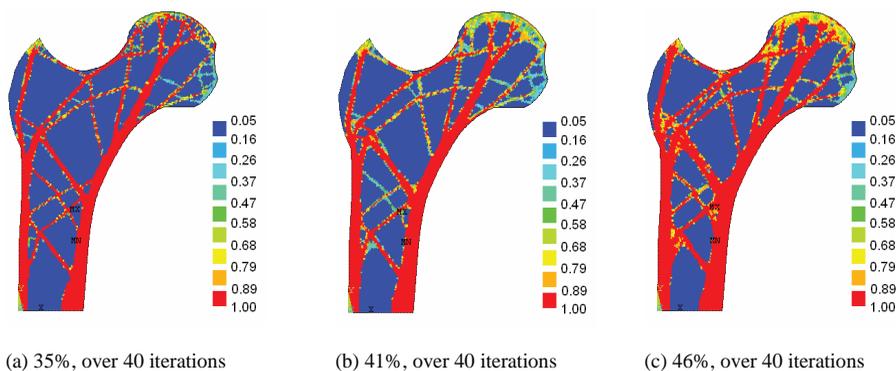
Figure 4: Isotropic material (*R*=1.0) distributions in proximal femur

Figure 4 displays the mass (relative density) distributions in a proximal femur when the total amount of material is different. It can be seen from Figure 4 that the material is placed mainly on the boundary of the lower part of proximal femur so as to give a stiffer structure for a given percentage of mass. Near the top of bone, the mass density also increases. Simultaneously, the distribution of material near the bottom of the bone forms a stiffer boundary for supporting loads, which applies to all three cases. Figure 4 also shows differences in mass distribution. In particular, the mass distribution in the mid-section for connecting the two vertical boundaries displays differences that are induced by the different percentages of mass specified. The two vertical sides have different amounts of material in each of the three cases.

4.2   Numerical results for bone with bi-modular material

In this example, *R* is assumed to be 0.2, 0.4 and 0.6 to investigate the effect of *R* on mass distribution in the femur. Figure 5 shows the distribution of relative density

(a) 35%, 33 iterations   (b) 41%, over 40 iterations   (c) 46%, over 40 iterations
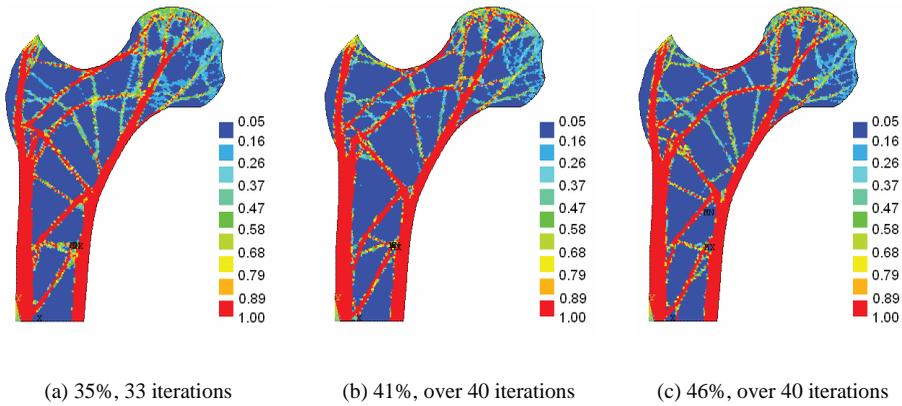
Figure 5: Material distributions for different volume percentages with R=0.2.

of bi-modular material in the proximal femur for different percentages of material and R=0.2 (i.e., the tension modulus is only 20% of the compressive modulus). Obviously, the number of elements with mid-density (relative density between 0.05 and 1.0) is greater than that for the case of isotropic material (see Figure 4). It is also seen from Figure 5 that the amount of mass near the left vertical side is much greater than that near the right vertical side. It can be concluded from Figure 5 that the material on the left side is mostly under tension state and the material near the right side is under compression state. Therefore, more material is required near the left side to support tension loads.

(a) 35%, over 40 iterations   (b) 41%, over 40 iterations   (c) 46%, 26 iterations
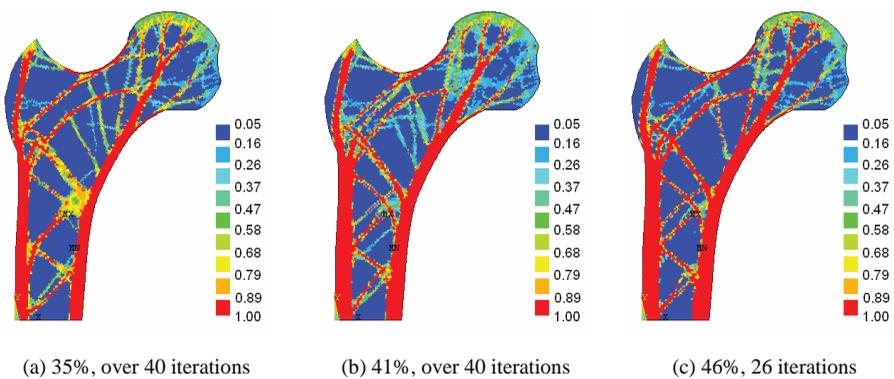
Figure 6: Material distributions for different structure with R=0.4.

Figure 6 presents a group of different material distributions in the femur for R=0.4.

Figure 6 shows that the material in middle part of the femur connecting the two sides is distributed differently in the three cases. For example, a higher percentage of mass (volume ratio) leads to more material being distributed on two sides. The reason is that the stiffness of femur will be improved obviously under current loads when more material is layout on the two vertical sides. Meanwhile, the amount of material under compression, i.e., near the right side, is nearly the same as that in the left side (under tension), which is different from the situation shown in Figure 5. The difference is mainly caused by the value of R, e.g., R=0.2 in Figure 5 and R=0.4 in Figure 6.

(a) 35%, over 40 iterations   (b) 41%, 31 iterations   (c) 46%, 20 iterations
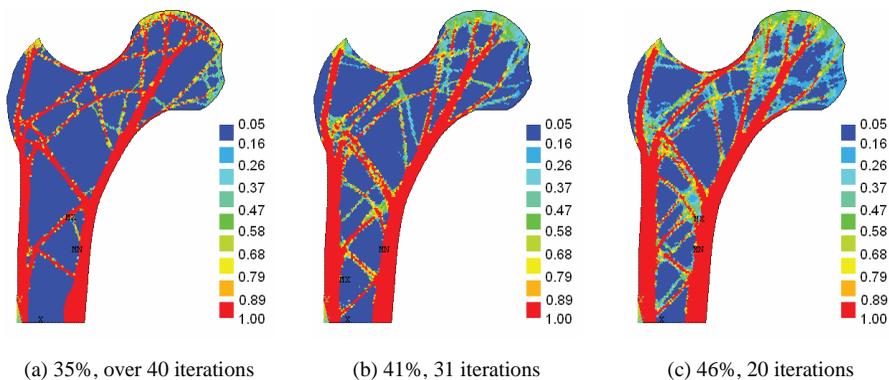
Figure 7: Material distributions for different percentage amount of mass R=0.6.

When R increases to 0.6, the difference between the two moduli is reduced. Therefore, the results are expected to be much closer to those in Figure 4 for the case of isotropic material, compared with those in Figure 5 and Figure 6. But the difference between Figure 7 and Figure 4 is still obvious for the mass distribution in the middle part of the femur. The similarity of the results in Figure 7b(with volume ratio of 41%) and Figure 7c (with volume ratio of 46%) implies that more mass is layout to connect the two vertical sides. Hence, the mass connecting the two vertical sides is more important than that connecting the top and the right side of the femur.

5   Conclusions

As a difference exists between the tensile modulus and the compressive modulus of either cortical bone or porous bone, it is important to investigate the effects of that difference on the mass distribution in the human proximal femur. The numerical results show that the mass distribution in a femur with bi-modular material is significantly different from those with isotropic material only. The amount of

mass near the two vertical sides (the left side is under tension and the right side is under compression) is affected by the difference between the two moduli, i.e., *R*. The topology algorithm developed here seems promising for determining optimal mass distribution of bones with bi-modulus and may provide guidance in developing therapy for osteoporosis with exercise methods as well as other applications in biomedical engineering. It should be mentioned that the real proximal femur is in fact a three-dimensional structure. The present results by using plane stress model are just showing the material layout in a longitudinal section of bone structure. In our future work, the three-dimensional material layout in a proximal femur will be considered.

References

1. Wolff, J. (1986) *The law of bone remodeling (Das Gesetz der Transformation der Knochen), Hirschwald, 1892 [Maquet P., Furlong R., Trans].* Springer: Berlin.

2. Cowin, S. C. (1986) Wolff's law of trabecular architecture at remodeling equilibrium. *Journal of Biomechanical Engineering-Transactions of the Asme* , 108, (1), 83-88.

3. Nazarian, A., Arroyo, F. J. A., Rosso, C., Aran, S. & Snyder, B. D. (2011) Tensile properties of rat femoral bone as functions of bone volume fraction, apparent density and volumetric bone mineral density. *Journal of Biomechanics* , 44, (13), 2482-2488.

4. Odgaard, A., Kabel, J., van Rietbergen, B., Dalstra, M. & Huiskes, R. (1997) Fabric and elastic principal directions of cancellous bone are closely related. *Journal of Biomechanics* , 30, (5), 487-95.

5. Qin, Q. H., Qu, C. Y. & Ye, J. Q. (2005) Thermo electroelastic solutions for surface bone remodeling under axial and transverse loads. *Biomaterials* , 26, (33), 6798-6810.

6. Qin, Q. H. & Ye, J. Q. (2004) Thermoelectroelastic solutions for internal bone remodeling under axial and transverse loads. *International Journal of Solids and Structures* , 41, (9-10), 2447-2460.

7. Qu, C. Y., Qin, Q. H. & Kang, Y. L. (2006) A hypothetical mechanism of bone remodeling and modeling under electromagnetic loads. *Biomaterials* , 27, (21), 4050-4057.

8. Whitehouse, W. J. & Dyson, E. D. (1974) Scanning electron microscope studies of trabecular bone in the proximal end of the human femur. *Journal of anatomy* , 118 (Pt 3), 417-44.

9. Qu, C. Y. & Qin, Q. H. (2006) Evolution of bone structure under axial and transverse loads. *Structural Engineering and Mechanics* , 24, (1), 19-29.

10. Hollister, S. J., Kikuchi, N. & Goldstein, S. A. (1993) Do bone ingrowth processes produce a globally optimized structure? *Journal of Biomechanics* , 26, (4-5), 391-407.

11. Fernandes, P., Rodrigues, H. & Jacobs, C. (1999) A model of bone adaptation using a global optimization criterion based on the trajectorial theory of Wolff. *Computer Methods in Biomechanics and Biomedical Engineering* , 2, (2), 125–138.

12. Bendsoe, M. P. & Kikuchi, N. (1988) Generating optimal topologies in structural design using a homogenization method. *Computer Methods in Applied Mechanics and Engineering* , 71, (2), 197-224.

13. Kowalczyk, P. (2010) Simulation of orthotropic microstructure remodelling of cancellous bone. *Journal of Biomechanics* , 43, (3), 563-569.

14. Kim, I. Y. & Kwak, B. M. (2002) Design space optimization using a numerical design continuation method. *International Journal for Numerical Methods in Engineering* , 53, 1979–2002.

15. Jang, I. G. & Kim, I. Y. (2008) Computational study of Wolff's law with trabecular architecture in the human proximal femur using topology optimization. *Journal of Biomechanics* , 41, (11), 2353-2361.

16. Cai, K., Chen, B. S., Zhang, H. W. & Shi, J. (2008) Stiffness design of continuum structures by a bionics topology optimization method. *Journal of Applied Mechanics-Transactions of the Asme* , 75, (5), 051006, 1-11.

17. Zhu, L., Zhao, H. P., Song, Y. L. & Feng, X. Q. (2006) Experimental investigation of the mechanical properties of Takin femoral cortical bone. *Journal of Tsinghua University (Sci & Tech)* , 46 (2), 301–304.

18. Cory, E., Nazarian, A., Entezari, V., Vartanians, V., Mueller, R. & Snyder, B. D. (2010) Compressive axial mechanical properties of rat bone as functions of bone volume fraction, apparent density and micro-ct based mineral density. *Journal of Biomechanics* , 43, (5), 953-960.

19. Cai, K., Gao, Z. & Shi, J. (2013) Compliance optimization of a continuum with bimodulus material under multiple load cases. *Computer-Aided Design* , 45, (2), 195-203.

20. Cai, K., Qin, Q. H., Luo, Z. & Zhang, A. J. (2013) Robust topology optimisation of bi-modulus structures. *Computer-Aided Design* , 45, (10), 1159-1169.

21. Medri, G. (1982) A non-linear elastic model for isotropic materials with different behavior in tension and compression. *Journal of Engineering Materials and Technology-Transactions of the Asme* , 104, (1), 26-28.

22. Victoria, M., Querin, O. M. & Marti, P. (2011) Generation of strut-and-tie models by topology design using different material properties in tension and compression. *Structural and Multidisciplinary Optimization* , 44, (2), 247-258.

23. Querin, O. M., Victoria, M. & Marti, P. (2010) Topology optimization of truss-like continua with different material properties in tension and compression. *Structural and Multidisciplinary Optimization* , 42, (1), 25-32.

24. Skedros, J. G. & Baucom, S. L. (2007) Mathematical analysis of trabecular 'trajectories in apparent trajectorial structures: The unfortunate historical emphasis on the human proximal femur. *Journal of Theoretical Biology* , 244, (1), 15-45.

25. Buchler, P., Ramaniraka, N. A., Rakotomanana, L. R., Lannotti, J. P. & Farron, A. (2002) A finite element model of the shoulder: application to the comparison of normal and osteoarthritic joints. *Clinical Biomechanics* , 17, (9-10), 630–639.

26. Qin, Q. H. & He, X. Q. (1995) Variational principles, FE and MPT for analysis of non-linear impact-contact problems. *Computer methods in applied mechanics and engineering* ,122, (3), 205-222.

27. Rozvany, G. I. N., Zhou, M. & Birker, T. (1992) Generalized shape optimization without homogenization. *Structural Optimization* , 4, (3-4), 250-252.

28. Xie, Y. M. & Steven, G. P. (1993) A simple evolutionary procedure for structural optimization. *Computers & Structures* , 49, (5), 885-896.

29. Wang, M. Y., Wang, X. M. & Guo, D. M. (2003) A level set method for structural topology optimization. *Computer Methods in Applied Mechanics and Engineering* , 192, (1-2), 227-246.

30. Bathe, K. J. (1996) *Finite element procedures*. Prentice-Hall, Inc. : New Jersey.

31. Jirousek, J., Wroblewski, A., Qin, Q. H. & He, X. (1995) A family of quadrilateral hybrid-Trefftz p-elements for thick plate analysis. *Computer Methods in Applied Mechanics and Engineering* , 127, (1), 315-344.

32. Qin, Q. H. (2000) *The Trefftz finite and boundary element method*. WIT Press: Southampton.

33. Qin, Q. H. (2003) Variational formulations for TFEM of piezoelectricity. *International Journal of Solids and Structures* , 40, (23), 6335-6346.

34. Qin, Q. H. (2005) Trefftz finite element method and its applications. *Applied Mechanics Reviews* , 58 (5), 316-337.

35. Bendsoe, M. P. & Sigmund, O. (2003) *Topology optimization: theory, methods, and applications*. Springer: Berlin, Heidelberg.

36. ANSYS (2013) *http://www.ansys.com (assessed March 2014)*.